Monthly Notices
of the
ROYAL ASTRONOMICAL SOCIETY

MNRAS **476,** 1258–1270 (2018)
Advance Access publication 2018 February 9

doi:10.1093/mnras/sty318

On the nature of the high-energy rollover in 1H 0419-577

T. J. Turner,[1,2]★ J. N. Reeves,[2,3] V. Braito[2,4] and M Costa[3]

[1]*Department of Physics, University of Maryland Baltimore County, Baltimore, MD 21250, USA*
[2]*Center for Space Science and Technology, University of Maryland Baltimore County, 1000 Hilltop Circle, Baltimore, MD 21250, USA*
[3]*Astrophysics Group, School of Physical and Geographical Sciences, Keele University, Keele, Staffordshire ST5 5BG, UK*
[4]*INAF - Osservatorio Astronomico di Brera, Via Bianchi 46, I-23807 Merate (LC), Italy*

Accepted 2018 February 2. Received 2018 February 1; in original form 2017 September 15

ABSTRACT

A *NuSTAR*/*Swift* observation of the luminous Seyfert 1 galaxy 1H 0419-577 taken during 2015 reveals one of the most extreme high-energy cut-offs observed to date from an AGN – an origin due to thermal Comptonization would imply a remarkably low coronal temperature $kT \sim 15$ keV. The low-energy peak of the spectrum in the hard X-ray *NuSTAR* band, which peaks before the expected onset of a Compton hump, rules out strong reflection as the origin of the hard excess in this AGN. We show the origin of the high-energy rollover is likely due to a combination of both thermal Comptonization and an intrinsically steeper continuum, which is modified by absorption at lower energies. Furthermore, modelling the broad-band XUV continuum shape as a colour-corrected accretion disc, requires the presence of a variable warm absorber to explain all flux and spectral states of the source, consistent with the previous work on this AGN. While absorber variations produce marked spectral variability in this AGN, consideration of all flux states allows us to isolate a colourless component of variability that may arise from changes in the inner accretion flow, typically at around 10 r_g.

Key words: galaxies: active – quasars: individual: 1H 0419-577 – galaxies: Seyfert – X-rays: galaxies.

1 INTRODUCTION

Observations with the *Ginga* satellite (e.g. Pounds et al. 1990) first measured a strong X-ray spectral component above 10 keV in type I active galactic nuclei (AGN), initially interpreted entirely as reflection of hard X-rays off cold, Compton thick matter in the form of an accretion disc.

However, X-ray measurements above 10 keV have been challenging both spatially and spectrally, leaving the detailed properties, and hence the origin of the hard X-ray flux open to debate. Scenarios involving partial covering of the continuum by Compton-thick matter (e.g. Turner et al. 2009) or Comptonization of soft seed disc photons (e.g. Mehdipour et al. 2011; Done et al. 2012; Di Gesu et al. 2014) have provided viable explanations for type I AGN.

A recent breakthrough in our understanding of the nature of the hard excess was made with *Suzaku*: Tatum et al. (2013) revealed that a majority of nearby type I AGN show a strong 'hard excess' above 10 keV, whereby the luminosity observed above 10 keV is too high to be explained by any models previously fit to the data below that energy. If interpreted in terms of absorption partially covering the line-of-sight, this would require that even the type I AGN are covered by low ionization Compton-thick matter, with columns in excess of $N_H > 10^{24}$ cm^{-2} covering at least 50 per cent of the central X-ray emission region. This is in contrast to what would be expected in AGN Unification Schemes (Antonucci 1993), where the sight-lines towards type I AGN are thought to be largely unobscured (see also Burtscher et al. 2016).

However, the observations may be explained if the obscuring medium is inherently clumpy (Elitzur & Shlosman 2006). Interest in clumpy reprocessor models has grown recently on the basis of data in many wavebands. Methods of testing models for the cloud ensemble have been explored using a Bayesian inference framework and applied successfully to Centaurus A (Asensio Ramos & Ramos Almeida 2009). Such clumpy models have also been applied to explain spectral energy distributions (SEDs; Alonso-Herrero et al. 2011; Asensio Ramos & Ramos Almeida 2013) and the IR properties of AGN (Ramos Almeida et al. 2014).

Popular models for AGN data below 10 keV have suggested the X-ray spectral form and variability below 10 keV can be explained by a partial-covering absorber (Pounds et al. 2004a,b, Terashima et al. 2009; Mizumoto, Ebisawa & Sameshima 2014) and so this hard X-ray model is a natural extension of that picture to higher column densities and energies. In such models, the absorption signature should be calculated along with the scattered (reflected) X-ray emission expected from clumps of the gas that lie out of the line of sight (e.g. Miller & Turner 2013). While the location of the Compton-thick component is not yet known, spectral variability

★ E-mail: tjturner@umbc.edu

time-scales show it to be consistent with an origin at or inside a clumpy obscuring torus. Possibilities within the torus include either an inhomogeneous disc wind or outflowing clouds that may be part of the optical broad-line region (e.g. Risaliti et al. 2007; Ricci et al. 2010). From consideration of the covering fraction and of the kinematics of X-ray absorbing gas, it seems likely that this zone may be part of a clumpy disc wind (Proga & Kallman 2004). Indeed, models for a Compton-thick wind (e.g. Proga & Kallman 2004; Sim et al. 2010) have shown promise to explain the hard X-ray form and Fe Kα emission of local Seyfert galaxies. Models by Sim et al. (2010) and Di Gesu et al. (2013) are examples of some of those that explore the line broadening that can be produced by such outflowing gas.

If, instead, the hard excess arises through X-ray reflection off Compton-thick matter out of the direct line of sight, then its strength measured by *Suzaku* in many AGN far exceeds what would be expected from a disc (or torus) subtending $\sim 2\pi$ sr. This model requires the intrinsic X-ray continuum to be heavily suppressed with respect to the reflected emission. This could be achieved if the trajectories of the individual continuum photons are curved away from the observer towards the plane of the disc due to the strong gravitational field of the black hole – subsequently this was referred to as the 'light-bending' model (Miniutti & Fabian 2004). Here, a strong, highly relativistically blurred reflection component can be produced which can dominate the intrinsic continuum above 10 keV. Application of this model to AGN spectral data, including 1H 0419-577, (Walton et al. 2013), required blurred reflection from material emitted predominantly from a few gravitational radii, around a maximal Kerr black hole to explain the hard excess (e.g. Fabian et al. 2005).

The Seyfert 1 galaxy, 1H 0419-577 ($z = 0.104$) provided the first report of the hard excess phenomenon (Turner et al. 2009) in *Suzaku* data and turned out to have typical X-ray absorber properties in the context of the later Tatum et al. (2013) study. 1H 0419-577 is also notable for having a highly variable X-ray spectrum in the 1–10 keV band, successfully parametrized in the past using variations in a complex X-ray absorber (Pounds et al. 2004a; Di Gesu et al. 2014). A correlated variability event in the X-ray and UV bands, studied using *XMM* data (Pal et al. 2017) helps motivate a broad-band study of the variability and spectral form of this AGN.

BeppoSAX provided the first evidence for 1H 0419-577 to have a flat component in the hard X-ray regime, (modelled in that case as a $\Gamma \sim 1.5$ powerlaw; Guainazzi et al. 1998); however, it was not until the *Suzaku* observations that this was identified as requiring a new Compton-thick absorption component, necessitating a revision of the intrinsic continuum level, and a paradigm-shifting reconsideration of the importance of Compton-thick absorption in type 1 AGN (Turner et al. 2009). Alternative parameterizations of the hard component as blurred reflection in 1H 0419-577, for example, Walton, Reis & Fabian (2010) and Pal & Dewangan (2013), require blurred reflection from a disc extending down to $\sim 1.4 r_{\rm g}$, with an emissivity index $q > 8$: the high degrees of blurring these models then reduce the disc component to a smooth continuum form.

Following on from *Suzaku*, *NuSTAR* has provided an opportunity for significant progress in understanding the hard spectrum of AGN, providing data with an unprecedented spatial resolution via imaging optics of 18 arcsec FWHM and spectral resolution 400 eV (FWHM) at 10 keV, along with a relatively high effective area up to ~80 keV. Thus, compared to previous non-imaging hard X-ray detectors, *NuSTAR* is not background dominated at energies above 10 keV and is able to provide sensitive measurements of the hard X-ray emission from AGN. Thus, *NuSTAR* affords an opportunity to disentangle the relative contribution of reflection, absorption as well as Comptonization to provide a self-consistent explanation for the shape of the broad-band data.

In this paper, we present an ~170 ks *NuSTAR* observation of 1H 0419-577. This observation was made with an overlapping exposure from *Swift* to enable a test of physically realistic models for the broad-band UV to hard X-ray continuum and reprocessing components in the target source. The primary motivation of the observations was to determine the relative importance of Compton thick absorption, reflection and Comptonization in shaping the hard X-ray emission from this AGN. Here, we also consider the archived *Suzaku* data to extend the XUV model to account for the marked spectral variability observed in 1H 0419-577 between different epochs (e.g. Guainazzi et al. 1998; Page et al. 2002; Pounds et al. 2004a). We also use the archived *XMM* observation that caught this source in an extreme low state (Pounds et al. 2004a), to test the extension of the final model across the full range of behaviour exhibited by this AGN.

2 OBSERVATIONS

2.1 NuSTAR

NuSTAR carries two co-aligned telescopes containing Focal Plane Modules A and B (FPMA, FPMB; Harrison et al. 2013) covering a useful bandpass of ~3–80 keV for AGN. *NuSTAR* observed 1H 0419-577 on 2015 June 3. Data were processed with HEASOFT 6.16 and the *NuSTAR* Data Analysis Software package v. 1.4.1. Event files were created through the NUPIPELINE task then calibrated with files from CALDB 20150316 and filtered using standard criteria.[1] Source and background spectra were extracted through regions of 50 arcsec radius then binned to 50 counts per spectral channel. This binning ensured sufficient counts in all channels for fitting using the chi-square statistic. After grouping, the data were still sampled more finely than the spectral resolution of the instruments. In the plots, the data are binned more coarsely than allowed in the fit, for visual clarity. The net exposure times were about 170 ks for each of FPMA and FPMB. FPMA gave 0.386 ± 0.002 ct s^{-1} from the source while FPMB gave 0.379 ± 0.002 ct s^{-1}, the background level was < 3 per cent of the total count rate. These rates correspond to a 10–50 keV flux 2.1×10^{-11}erg cm^{-2}s^{-1}. Examination of the *NuSTAR* images confirmed that no strong hard X-ray source exists that would have compromised the measurement of the hard X-ray spectrum in previous PIN (e.g. Turner & Miller 2009) or *BeppoSAX* PDS observations (Deluit & Courvoisier 2003) of 1H 0419-577.

2.2 Swift

Swift observations were obtained 2015 June 3–9 (OBSID 00081695001), simultaneous with the *NuSTAR* observation. The *Swift* X- Ray Telescope (XRT; Burrows et al. 2005) observations totaled 4.1 ks and were performed in photon counting mode. The data were reduced using HEASOFT 6.13 with XRTPIPELINE v 0.13.2. Source and background photons were extracted using XSELECT version 2.4c, from circular regions with radii of 47 arcsec and 189 arcsec, respectively. The XRT yielded a source count rate of 0.48 ± 0.01 ct s^{-1}, and the background rate was < 0.5 per cent of the total. Pileup

[1] Upon revision of the paper, we re-extracted the *NuSTAR* data with the latest HEASOFT (v6.22) and the *NuSTAR* CALDB dated 20170817 and found that the spectra were consistent within errors with the original spectral products extracted in 2015.

is negligible in these data. The spectral data were re-binned to have at least 25 photons per bin (still sufficient for application of the chi-squared statistic, but in this case, application of a higher photon count per bin would have reduced the spectral resolution of the data.)

The *Swift* UV-optical Telescope (UVOT; Roming et al. 2005) was used with the *U*-band filter, that was the only UV data simultaneous with the 2015 X-ray data. The *U* filter has a central wavelength 3465 Å. Source photons were selected from a circle of radius 5 arcsec, yielding a count rate 81.64 ± 1.81 ct s^{-1}. The sky background was <4 per cent of the total count rate. Using the host galaxy template of (Bentz et al. 2009), and following their relation between galaxy luminosity and the 5100 Å luminosity of the AGN, we scaled the host template to the 5100 Å flux of 1H 0419-577 and from that we estimated the contamination from the host galaxy to be at the ∼2 per cent percent level in the *U* band, and therefore negligible.

2.3 Suzaku

Four *Suzaku* telescopes focus X-rays on to the X-ray Imaging Spectrometer CCD array (XIS; Koyama et al. 2007; Mitsuda et al. 2007). XIS units 0,2,3 are front-illuminated (FI) and cover ∼0.6–10.0 keV with energy resolution FWHM ∼150 eV at 6 keV. XIS2 developed a charge leak in 2006 November, and has not been used since then. XIS 1 is a back-illuminated CCD, giving it an enhanced soft-band response, extending down to 0.2 keV but this has a lower effective area at 6 keV than FI CCDs and has a higher background level at high energies. *Suzaku* also carries a non-imaging, collimated Hard X-ray Detector (HXD; Takahashi et al. 2007), whose PIN instrument provides useful AGN data in the ∼15–70 keV band.

The *Suzaku* observations of 1H 0419-577 were made 2007 July 25 (OBSID 702041010) and 2010 January 16 (OBSID 704064010). During the 2007 observation the source was observed at the nominal centre position for the XIS, during the 2010 observation it was observed at the nominal centre position for the HXD. We ran the pipeline processing using HEASOFT v 6.16 and CALDB 20150316, following the standard reduction as previously published for the 2007 observation, detailed by Turner & Miller (2009).

The summed exposure time was 411 ks for the FI CCDs during 2007, and 246 ks during 2010. XIS spectra and light curves were extracted from circular regions of radius 2.9 arcmin with background spectra extracted from a region of the same size but offset from the source and avoiding chip corners where calibration source data are recorded. Data in the range 1.78–1.9 keV were excluded from XIS due to uncertainties in calibration around the instrumental Si K edge. The background level was 1 per cent of the total XIS count rate.

1H 0419-577 is too faint to be detected in the HXD GSO instrument, but was detectable in the PIN. The PIN data reduction and a comparison of two methods of PIN background estimation reduction are detailed by Turner & Miller (2009), and here we followed that method and used the model 'D'. PIN background.[2] The net PIN exposures were 142 and 105 ks during 2007 and 2010, respectively. 1H 0419-577 comprised ∼15 per cent of the total source-plus-background counts in the PIN band. For *Suzaku*, spectral fits used the only operational FI CCDS, XIS 0 and 3 over 0.6–10 keV and PIN data in the energy range 15–40 keV. (XIS1 was not used owing to the relatively high background level at high energies.)

[2] http://www.astro.isas.jaxa.jp/suzaku/doc/suzakumemo/suzakumemo-2007-01.pdf

During 2007 1H 0419-577 yielded full-band (0.6–10 keV XIS and 15–70 keV PIN, background subtracted) count rates 1.157 ±0.002 (per XIS unit) and $3.053 \pm 0.13 \times 10^{-2}$ (PIN) ct s^{-1} corresponding to a 0.5–2 keV flux 1.5×10^{-11}erg cm^{-2} s^{-1}, 2–10 keV flux 1.8×10^{-11}erg cm^{-2} s^{-1} and 10–50 keV flux 2.9×10^{-11}erg cm^{-2} s^{-1}, consistent with the hard flux measured by *NuSTAR* when mission and instrument cross calibration uncertainty is taken into account.

During 2010 the rates were 0.790 ±0.002 (per XIS) and $2.71 \pm 0.15 \times 10^{-2}$ (PIN) ct s^{-1} corresponding to a 0.5–2 keV flux 1.2×10^{-11}erg cm^{-2} s^{-1}, 2–10 keV flux 1.4×10^{-11}erg cm^{-2} s^{-1}, and 10–50 keV flux 2.4×10^{-11}erg cm^{-2} s^{-1}.

2.4 *XMM–Newton*

XMM–Newton (hereafter *XMM*) captured 1H 0419-577 in a historical low state during 2002 September (OBSID 0148000201). The flux range observed with *XMM* (Page et al. 2002; Pounds et al. 2004a) was $0.2–1.3 \times 10^{-11}$ erg cm^{-2} s^{-1} in the 0.5–2 keV band and $0.9–1.6 \times 10^{-11}$ erg cm^{-2} s^{-1} in the 2–10 keV band.

The EPIC pn spectrum plus the OM *U*-band filter data extracted via SAS v16 were used as a test of the extension of the model to the most extreme flux states. As the optical and ultraviolet fluxes are variable by up to 30 per cent for 1H 0419-577 (e.g. Pal et al. 2017), we chose only the simultaneous *U*-band photometry point from the OM data, for the most meaningful comparison.

Following Page et al. (2002) the data were screened to limit acceptable event patterns to the range 0–4. Hot and bad pixels were removed. Source counts were obtained from a circular region of 45 arcsec radius centred on 1H 0419-577, with the background being taken from a similar region on the same chip but offset from the source. Periods of high background were removed from the observation. The resultant spectrum had a net exposure of 12 ks. The pn spectrum was binned to a minimum of 50 counts per energy bin and the binned data maintained sampling finer than the spectral resolution of the pn.

3 SPECTRAL FITTING RESULTS

The full-band *Suzaku* XIS light curve showed <40 per cent flux variability during 2007 and 2010. The source flux variations were <20 per cent during the *NuSTAR* observation. The source has previously been reported as showing a steady light curve during the *XMM* observation of 2002 September (Pounds et al. 2004b). Thus, in this paper we report only the mean spectra from each epoch observed.

Spectra are analysed with XSPEC v12.9.0. All errors correspond to 90 per cent confidence levels for one parameter of interest.

3.1 Cross calibration and grouping

When performing joint *NuSTAR* fits with the *Swift* XRT and UVOT data, we used *NuSTAR* data over 3–70 keV, and *Swift* XRT over 0.3–6.0 keV. We introduced a multiplicative factor to account for differences in the relative flux calibrations of the various instruments. Fixing a constant model parameter to 1 for FPMA, we allowed the normalization of FPMB and the *Swift* XRT and *U*-band spectral files to vary relative to that. For the 2015 data, we found the cross-normalization factor was <5 per cent between the 2015 data sets, and so we then constrained the relative normalizations to lie within that range, because this later sped up the more complex multi-epoch fitting.

In the spectral model, the PIN model flux was increased by a factor 1.16 for 2007 and 1.17 for 2010, as recommended, to account for the instrument cross-calibration at the epoch of those observations (and these cross calibration factors were fixed in the fit).[3] XIS data were binned at the HWHM resolution for each instrument while PIN data were binned to be a minimum of 5σ above the background level for the spectral fitting. Note that as the PIN data are of much lower signal to noise compared to *NuSTAR*, in the subsequent plots we have binned the PIN data to give a single flux point compared to the *NuSTAR* spectra.

For *XMM*, the EPIC pn spectrum plus the OM *U*-band filter data extracted via SAS V16 were used as a test of the extension of the model to the most extreme flux states. A 10 per cent error was applied to the OM U flux, to account for the flux calibration uncertainty of the OM.[4]

3.2 Basic parametrization of the broad-band spectral form

A full covering screen of neutral gas was included in all fits presented in this paper, to represent the Galactic line-of-sight column density $N_{\rm H} = 1.26 \times 10^{20}$ atoms cm^{-2}, parametrized using TBABS. We also accounted for the UV extinction of $E(B-V) = 0.0186$ from Cardelli, Clayton & Mathis (1989) using the REDDEN model. In XSPEC, the transmission is set to unity short-ward of the Lyman limit, allowing REDDEN to be used in combination with TBABS in the fit.

The flux observed for 1H 0419-577 during the 2015 observation corresponds to an observed luminosity $L_{2-10} = 4.1 \times 10^{44}$ erg s^{-1} (assuming $H_0 = 70$ km s^{-1} Mpc^{-1}).

First, we attempted to make a basic characterization of the broad-band XUV spectral form during the 2015 campaign, to extract a simple phenomenological parametrization of the spectral energy distribution. To this end, we applied a simple double broken power-law model to the 2015 *NuSTAR* plus *Swift* data over 0.3–79 keV. This provided a good fit to the data with a $\Gamma \sim 2.4$ slope joining the *U*-band point to the soft X-ray data (Fig. 1). At 1 keV, this flattens to a $\Gamma \sim 1.7$ slope continuing up to ∼20 keV. In the 20–50 keV range the spectrum steepens again, to $\Gamma \sim 2.2$, appearing to recover the slope of the soft X-ray to UV portion of the spectrum. For this epoch, the observed $\alpha_{\rm ox} \sim 1.76$.

We also attempted a simple parametrization of the Fe K emission line, known to be weak (Turner & Miller 2009), to guide our subsequent model selection. The *Suzaku* XIS data yield the best constraints on Fe K emission (Fig. 2). Measuring the line equivalent width relative to a 'local' power-law continuum (fitted over 3–10 keV), we fit the line with a Gaussian model, obtaining a reduction in fit statistic $\Delta\chi^2 \sim 54$ for three additional degrees of freedom (giving $\chi^2 = 223.7/208$ degrees of freedom). The fitted line energy was $E_{\rm Fe} = 6.34 \pm 0.06$ keV, width $\sigma < 380$ eV, and equivalent width 31^{+34}_{-10} eV (Fig. 2). Applying the same model to the *NuSTAR* data yields a line equivalent width 55 ± 15 eV for a width fixed at $\sigma = 100$ eV.

3.3 Comptonization models

The simple double broken power-law parametrization of the data has characterized the basic spectral shape of the source,

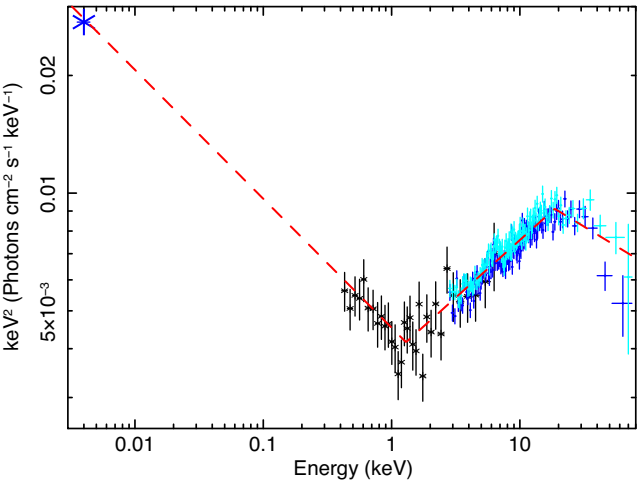

Figure 1. The simultaneous *NuSTAR* and *Swift* SED of 1H 0419-577. A double broken power-law model (red dashed line) has been fitted to the 2015 data, showing the *Swift* UVOT (*U* band, dereddened, dark blue star) and XRT (black cross) data, along with the *NuSTAR* FPMA (dark blue cross) and FPMB (aqua cross). Note the hard X-ray continuum ($\Gamma = 1.7$) up until a break energy of 20 keV, above which the spectrum significantly steepens ($\Gamma = 2.2$). A strong UV to soft X-ray excess is present below 1 keV.

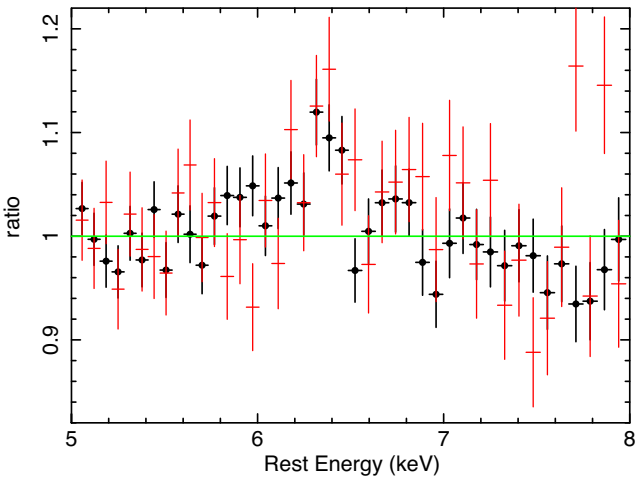

Figure 2. Suzaku XIS 0 3 data in the Fe K regime: 2010 (red) and 2007 (black) compared to a local power-law continuum model over 5–8 keV. A weak, but narrow, iron Kα emission line is seen near to 6.4 keV in the QSO rest frame.

and suggests that a broad-band continuum model should be applied, that allows for spectral steepening above 20 keV, similar to those observed previously for AGN in *BeppoSAX* data (e.g. Dadina 2008). To investigate the high-energy spectral roll over, we modelled the spectrum using Comptonization models (e.g. Petrucci et al. 2001).

As a previous *XMM*, RGS exposure of 1H 0419-577 has detected soft-band line emission from C, N, O, and Ne (e.g Pounds et al. 2004a; Di Gesu et al. 2013), we need to account for that gas before trying to constrain the continuum form. Detailed analysis of the RGS data led Di Gesu et al. (2013, using the SPEX code) to suggest that the X-ray emitter resides on pc size scales. To account for the line emission from that gas, we included in the model and all

[3] ftp://legacy.gsfc.nasa.gov/suzaku/doc/xrt/suzakumemo-2008-06.pdf
[4] http://xmm2.esac.esa.int/docs/documents/CAL-TN-0019.pdf

subsequent models an XSTAR table at the systemic redshift of the host galaxy. The emission line table was generated using XSTAR v 2.2.1 with a turbulent velocity 300 km s^{-1} and an illuminating spectrum consistent with the SED characterization (Section 3.2). The XSTAR table assumed a density $n = 10^{12}$ cm^{-3}, and we note that the emergent spectrum calculated by XSTAR is not sensitive to the density at the spectral resolution available from *NuSTAR* and the *Swift* XRT.

An initial fit of the soft-band XRT spectrum shows that our data do not allow new insight into the soft-band X-ray emitter, but are consistent with the previous results from RGS. As the column density and normalization of this component are degenerate, we fixed the column at 10^{21}atoms cm^{-2} for the fit (i.e. in the middle of the range fitted by Di Gesu et al. 2013) and allowed the normalization to be free. An initial fit to the 0.3–2.0 keV band alone yielded an ionization parameter $\log \xi = 1.30 \pm 0.51$ (where $\xi = \frac{L}{nr^2}$ and L is the ionizing luminosity integrated from 1 to 1000 Ryd, n is the proton density and r the distance of the material from the central black hole). This value of ξ was fixed for the soft emitter, in subsequent fits. We also note that some of the narrow soft-band emission lines could arise from a distant scattering/reflection component.

The Fe Kα emission line observed is stronger than that which could be produced by the soft-line emitting gas, and so a Gaussian line component was initially added to the fit to account for that. Note that in subsequent fits the Fe Kα emission is self-consistently fitted using ionized reflection models.

With these components in place, we constructed two variations on a simple Comptonization model. Both versions used COMPTT to describe the soft X-ray band, this is an analytic model describing Comptonization of soft photons in a hot plasma (Titarchuk 1994). Then the hard part of the spectrum was tested against two alternative models, a second COMPTT component or a thermally Comptonized continuum, available in XSPEC as NTHCOMP (Zdziarski, Johnson & Magdziarz 1996; Życki, Done & Smith 1999). The free parameters of NTHCOMP are the temperature of the corona, the soft-photon temperature and the power-law index of the spectrum. The advantage of NTHCOMP over COMPTT is that the seed photons in COMPTT are limited to have a blackbody distribution, those in NTHCOMP can be chosen to have a multicolour disc distribution. The *Swift* U-band point was omitted from these fits, as neither the COMPTT nor NTHCOMP models extend into the UV region as implemented in XSPEC.

We assumed a plasma temperature of 2 keV to account for the soft part of the spectrum, and obtained a fitted optical depth $\tau = 1.9^{+0.4}_{-0.5}$ for that cool zone. For the hard X-ray band, parametrization as COMPTT, using an input blackbody temperature of 10 eV (reasonable for a black hole of this mass, accreting at high efficiency) yields a plasma temperature $kT = 15.1 \pm 0.8$ keV, $\tau = 2.5 \pm 0.1$, ($\chi^2 = 957/949$ degrees of freedom), while NTHCOMP yields $kT = 13.4 \pm 1.0$ keV and a photon index $\Gamma = 1.74 \pm 0.01$, ($\chi^2 = 946/949$ degrees of freedom).

While these are good fits from a statistical perspective, the fitted temperatures are extremely low, yet conversely the photon index is unusually hard and thus the overall spectral form may not be viable for an AGN. There is also a concern that the low fitted temperature might be an artefact of the spectral curvature from the known absorber in this AGN, which can modify the continuum so that the observed photon index is much flatter below 10 keV compared to the steeper ($\Gamma > 2$) primary continuum which emerges at higher energies. Indeed, detailed modelling of the spectral form and marked spectral variability sampled over a large body of X-ray data for 1H 0419-577 provide compelling evidence for the presence of a variable, partial-covering absorber (e.g. Pounds et al. 2004a,b; Page et al. 2002) comprising at least two zones of ionized gas.

3.4 Reflection Modelling

In order to test the applicability of the popular reflection model, we then tested if the higher energy spectral curvature in the *NuSTAR* data as well as the soft continuum seen in *Swift* XRT could be explained by an ionized reflector. To this end we first fit the spectra using the most recent version of the RELXILL blurred disc reflection model (Garcia et al. 2014), which convolves the XILLVER reflection model (Garcia et al. 2013) with the relativistic RELLINE code (Dauser et al. 2014). We assumed Solar abundances and linked the illuminating photon index to that of the primary power-law. We fit the model over the 3–79 keV range of the NuSTAR data and the ∼0.4–5 keV band of the *Swift* XRT.

Among the several flavours of the model, we first tested the standard version of RELXILL, which allows the user to vary the high-energy cut-off, which can then be linked to the cut-off energy of the primary power law. The photoionized emitter, previously required to fit the narrow line emission in the soft X-ray band, is also retained in the model. We fixed the black hole spin to $a = 0.998$ (which otherwise is not constrained) and found that the model accounts well for the overall spectral shape (see Fig. 3, upper panel), with an overall fit statistic of $\chi^2_\nu = 940.1/949$. The reflection parameters yield an ionization state of $\log \xi = 2.70^{+0.04}_{-0.30}$ erg cm s^{-1}, a hard photon index of $\Gamma = 1.64 \pm 0.04$ and a disc inclination of $\theta = 26^{+9}_{-8}$. We note that the model is not dominated by the reflection component and the flux ratio between the reflector and the direct power law is relatively low, with $R = 0.21^{+0.11}_{-0.10}$ as measured over the 10–50 keV band. The reflector does not require a high degree of blurring, with an emissivity index of $q = 1.98^{+1.23}_{-1.56}$. However, the fit still requires the presence of relatively low cut-off energy, $E_{\rm cut} = 63^{+8}_{-9}$ keV. If we fix the cut-off energy at $E_{\rm cut} = 300$ keV, the fit is worse by $\Delta\chi^2 = 60.4$. We also checked alternative reflection scenarios where the higher energy rollover is a signature of a highly blurred and strong reflector, but generally these models require a low iron abundance (<0.55 × Solar) and a rather high emissivity ($q > 6$), in order to explain the smooth high-energy continuum curvature and the lack of a strong Fe Kα emission line. However, such blurred reflection models can account for the soft X-ray excess that is present and a separate soft X-ray continuum component modelled with COMPTT is no longer required in this particular case. Furthermore, these fits are significantly worse and can be rejected compared to the case above.

Given the low emissivity index for the above reflection fit and the relatively narrow width of the iron Kα line (e.g. as implied by the previous Gaussian fits), we also tested whether the spectrum can be simply modelled using an unblurred reflector originating from scattering off more distant material. To test this, we replaced the RELXILL model with a XILLVER ionized reflection table (Garcia et al. 2013), with a variable cut-off energy, which simulates the angle averaged reflection spectrum of a power-law illuminating a plane-parallel and optically thick slab. We assumed Solar abundances and again linked the illuminating photon index and high-energy cut-off of the reflector to that of the primary hard X-ray power law. The fit statistic is again very good, with $\chi^2_\nu = 934.2/950$, statistically equivalent to the blurred reflection fit and can account for the overall shape of the broad-band spectrum (see Fig. 3, lower panel). Again the primary power law has a rather hard photon index ($\Gamma = 1.52 \pm 0.12$)

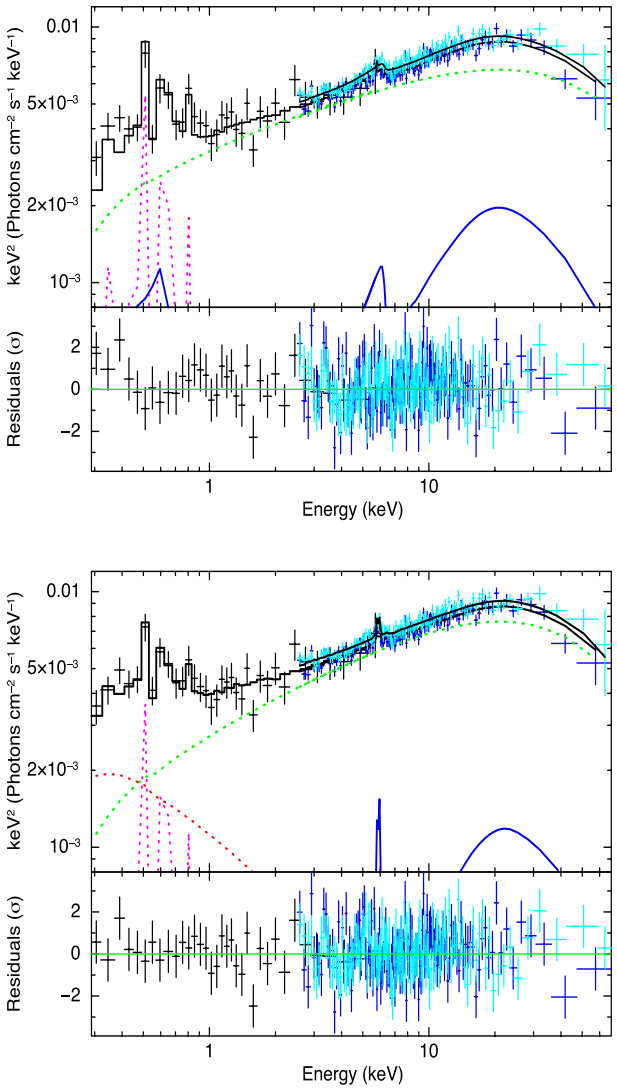

Figure 3. Data, model and residuals to joint fits to the *NuSTAR* (FPMA dark blue, FPMB aqua)/*Swift*(black cross) data. Top: (a) The model comprises a power-law continuum (green dashed line) and photoionized emitter (magenta dashed line) with blurred reflection modelled using RELXILL (dark blue solid line) with the cut-off energy allowed to be free. Bottom: (b) the reflection model, without relativistic blurring (i.e modelled using XILLVER without convolution with RELLINE). Model components as for (a), with the addition of a COMPTT, shown as a red dashed line. See Section 3.4 for details.

and requires a low cut-off energy of $E_{\rm cut} = 44^{+11}_{-12}$ keV to model the rollover at high energies. The reflector has an ionization state of $\log \xi = 2.3 \pm 0.4$, while its contribution is also weak compared to the power law; measured over the 10–50 keV band the flux ratio is $R \sim 0.12$. Note that unlike for the blurred reflection model, an additional soft continuum component modelled using the COMPTT model, is required to account for the soft excess in the *Swift* data, as noted in previous analysis (Pal & Dewangan 2013). In this case, the electron temperature of this soft Comptonization component has been fixed at $kT = 1$ keV and has an optical depth of $\tau = 4.5 \pm 1.2$.

We conclude that while reflection models give a good account of the broad-band X-ray spectrum of 1H -410-577, they cannot explain the hard X-ray curvature without a value for the high-energy cut-off that lies within the *NuSTAR* bandpass. We find that the fitted cut-off is lower than typical values in many AGN (Fabian et al. 2015). Furthermore, either a moderately blurred or a distant reflector can equally provide an acceptable fit of the reflection features in the data and thus highly blurred reflection is not required to model the broad-band spectrum. To understand this source, we need to consider physical models that can fit the underlying UV to X-ray continuum, as well as to investigate the effect of any absorption on the primary continuum emission, which can impart significant spectral curvature upon the primary continuum. We now consider this in the next Section.

3.5 The OPTXAGNF model

To account for the broad-band UV to X-ray continuum form using an accretion disc framework, we then turned to the OPTXAGNF model (Done et al. 2012). In this model, the gravitational energy released in the accretion disc is emitted as a blackbody with colour–temperature correction, whose temperature depends on radius. This blackbody extends to the so-called 'coronal radius', $R_{\rm cor}$ (expressed in gravitational radii, $r_{\rm g} = \frac{GM}{c^2}$, where M is the mass of the black hole in solar masses, G is the gravitational constant, and c is the speed of light). Below $R_{\rm cor}$ the system energy cannot fully thermalize and is distributed between low-energy and high-energy electron populations, giving rise to soft and hard Comptonization components, forming the so-called soft excess and hard-band power law, respectively. The hard Comptonization component is parametrized by a power-law with cut-off energy of 100 keV. Done et al. (2012) normalize the model by $\frac{\cos i}{\cos 60^\circ}$ as the optical emission is fairly isotropic for inclination angles $i < 60^\circ$. The OPTXAGNF model is compelling because it allows us to make a physically meaningful connection between the UV and X-ray emission, sampled by the simultaneous *NuSTAR* and *Swift* data. As the Galactic line-of-sight column is low in the direction of 1H 0419-577, this object is well-suited for fitting with a broad SED model such as OPTXAGNF.

OPTXAGNF assumes the two Comptonization regions to be geometrically co-spatial and that the maximum temperature of the disc is that at $R_{\rm cor}$ (Table 1). The model is angle-averaged, corresponding to an inclination angle of 60°. Input parameters for the model are the nuclear black hole mass and the distance to the source, the black hole spin, the bolometric Eddington ratio $\frac{L}{L_{\rm Edd}}$, $R_{\rm cor}$ and the outer disc radius, the electron temperature and optical depth of the low-energy electron population, the power-law index of the high-energy emission and the fraction of the power below the coronal radius which is emitted in the hard Comptonization component, $f_{\rm PL}$. The model normalization is frozen at 1.0 in the fit, as the model flux is determined by the combination of black hole mass, spin, Eddington ratio and the galaxy distance. Mass estimates for this source range from 1.3×10^8 M$_\odot$ (Pounds et al. 2004b) to 3.8×10^8 M$_\odot$ (O'Neill et al. 2005). We have adopted 3.8×10^8 M$_\odot$ for use in the OPTXAGNF fits, and this has a corresponding Eddington luminosity $L_{\rm Edd} = 4.6 \times 10^{46}$ erg s^{-1}. We take the comoving radial distance of the source to be 418 Mpc.[5] The electron temperature was limited to be <1 keV for the soft Comptonizing region (to maintain a distinction between the soft and hard Comptonizing regions in the fit and to restrict the fit to a meaningful parameter regime). During fitting, we found that kT hit the limit of 1.0 keV and so it subsequently was fixed at that value, which may be typical for AGN. For comparison, such models have recently been applied successfully to Ark 120, where Porquet et al. (2017) find a good fit with temperature

[5] ned.ipac.caltech.edu

Table 1. Variable Eddington ratio with partial ckovering.

Component	Parameter	2015[a]	2015	2010	2007	2002
		NuSTAR/Swift	NuSTAR/Swift	Suzaku	Suzaku	XMM (low)
	L^{b}_{2-10}	4.12	4.12	3.84	4.77	2.31
	L^{c}_{2-10}	6.66	6.66	6.79	8.43	6.35
OPTXAGNF	Γ	2.04 ± 0.03	1.99 ± 0.03	1.99^{t}	1.99^{t}	1.99^{t}
	$\log \frac{L}{L_{\rm Edd}}^{d}$	$-0.45^{+0.16}_{-0.26}$	$-0.45^{+0.08}_{-0.13}$	$-0.39^{+0.07}_{-0.12}$	$-0.37^{+0.06}_{-0.09}$	$-0.42^{+0.22}_{-0.23}$
	$R_{\rm cor}$	$15.9^{+47.0}_{-11.1}$	$16.4^{+50.0}_{-12.2}$	16.4^{t}	16.4^{t}	16.4^{t}
	τ	$3.10^{+0.57}_{-1.94}$	$5.47^{+0.29}_{-1.07}$	5.47^{t}	5.47^{t}	5.47^{t}
	f^{c}_{pl}	$0.14^{+0.28}_{-0.24}$	$0.14^{+0.09}_{-0.08}$	0.14^{t}	0.14^{t}	0.14^{t}
ZXIPCF$_1^{e}$	$N_{\rm H}$	$3.77^{+1.29}_{-0.60}$	$3.72^{+0.46}_{-0.51}$	3.72^{t}	3.72^{t}	$1.79^{+1.29}_{-1.11}$
	$\log \xi$	$0.43^{+0.83}_{-0.30}$	$0.66^{+0.32}_{-0.29}$	0.66^{t}	0.66^{t}	$-0.37^{+0.20}_{-0.15}$
	$f^{f}_{\rm cov}$	$0.34^{+0.11}_{-0.20}$	$0.42^{+0.03}_{-0.05}$	0.34 ± 0.03	0.34^{t}	$0.50^{+0.12}_{-0.09}$
ZXIPCF$_2^{e}$	$N_{\rm H}$	0.30 ± 0.55	$0.17^{+0.11}_{-0.09}$	0.17^{t}	0.17^{t}	$0.65^{+0.50}_{-0.42}$
	$\log \xi$	<0.15	0.00 ± 0.50	0.00^{t}	0.00^{t}	$-1.26^{+0.33}_{-0.87}$
	$f^{f}_{\rm cov}$	$0.34^{+0.18}_{-0.06}$	$0.57^{+0.04}_{-0.06}$	0.31 ± 0.07	0.31^{t}	$0.88^{+0.08}_{-0.07}$
χ^2/ degrees of freedom		925/945		1432/1312		1857/1634

Notes. A column of neutral gas covered all components, fixed at the Galactic value $N_{\rm H} = 1.26 \times 10^{20}\,{\rm cm}^{-2}$. ^{t} indicates that a parameter was tied to the other epochs during fitting. *p* indicates the parameter pegged at one of the limits. Errors are calculated at 90 per cent confidence. Reflection was modelled using XILLVER. See the text for model details.

[a]The 2015 fit was repeated allowing the column densities and ionization parameters to be free of constraint from the other epochs.

[b]The observed 2–10 keV luminosity in units of 10^{44} erg s^{-1}.

[c]The absorption-corrected 2–10 keV luminosity in units of 10^{44} erg s^{-1}.

[d]The units for log ξ are erg cm s^{-1}.

[e]Column density in units of 10^{23} atom cm^{-2}.

[f]Percentage covering.

$kT = 0.5$ keV and optical depth $\tau \sim 9$ to explain the soft excess (also see Różańska et al. 2015, and references within).

The black hole spin is degenerate with other parameters, and so we restricted our investigation of spin to a comparison of fits with spin set at the maximum and minimum values of $a = 0.998$ and $a = 0.0$, respectively. The fit with spin = 0.998 was favoured at > 99.99 per cent confidence for all variations of fit that are presented in this paper, therefore only the maximal spin fits are tabulated here (Tables 1–3). However, we caution that while our model constraints offer an interesting case study, we cannot rule out other solutions that combine different model assumptions with a low black hole spin. Other parameter degeneracies exist. For AGN soft excesses in general, the temperature of the soft X-ray emitting plasma parametrized as kT, is degenerate with the optical depth, τ. So if kT is increased in the model then τ will decrease in the fit to compensate (and vice versa), because overall, the luminosity or spectral shape will remain approximately the same. We note that some of the other degeneracies of the OPTXAGNF model are discussed by Thomas et al. (2016). Those authors discuss the practical application of the OPTXAGNF model, noting the complete degeneracy between the black hole mass and luminosity and they discuss how the spectral shape of the AGN SED can be described by three non-degenerate parameters, the energy of the peak of the accretion disc emission, the photon index of the non-thermal emission and the fraction of the total flux that is emitted in the non-thermal component.

To account for the Fe K line, we again included a reflection component from the XILLVER model, with the assumptions generally set as in the reflection fits of Section 3.4. The high-energy cut-off of the reflector was assumed to be 100 keV for consistency with the rollover built into the OPTXAGNF model. Importantly, here we did not convolve the reflector with any gravitational blurring, given both the narrow Kα line width and flat emissivity profile found previously. The soft line emission table was also added to the model, as previously described.

Fitting this OPTXAGNF plus XILLVER model to the simultaneous *NuSTAR* and *Swift* data from 2015 we found that even upon the inclusion of ionized reflection in the model, the overall OPTXAGNF fit overpredicts the *NuSTAR* flux in the hard X-ray band above 10 keV, while pronounced curvature is still present and the fit is still poor ($\chi^2 = 1117/953$ degrees of freedom, see Fig. 4). This is due to the fact that continuum fit is driven by the relatively hard portion of the SED between 2 and 10 keV (as shown in Fig. 1), which requires a relatively hard photon index of $\Gamma = 1.8$, while the spectral slope in the hard band above 10 keV is much steeper ($\Gamma > 2$). The reflection component in the model only contributes towards a maximum of 10 per cent of the total flux in the hard band and increasing its strength further leads to a substantially worse fit, as the hard flux then becomes even more discrepant with what is predicted by the model. Thus, the broad-band spectrum of 1H 0419-577 is not likely to be dominated by a strong reflection component, given both the weak Compton hump that is present and the lack of any strong iron Kα emission, as described earlier. Of course, the reflection component that we use here can arise from any Compton thick gas, it is not necessarily from the accretion disc and indeed, we later suggest that it may arise from clumps of material associated with the thick zone of absorption, seen out of the line of sight.

This suggests that either the intrinsic continuum is more complex in form and/or a substantial column of line of sight material

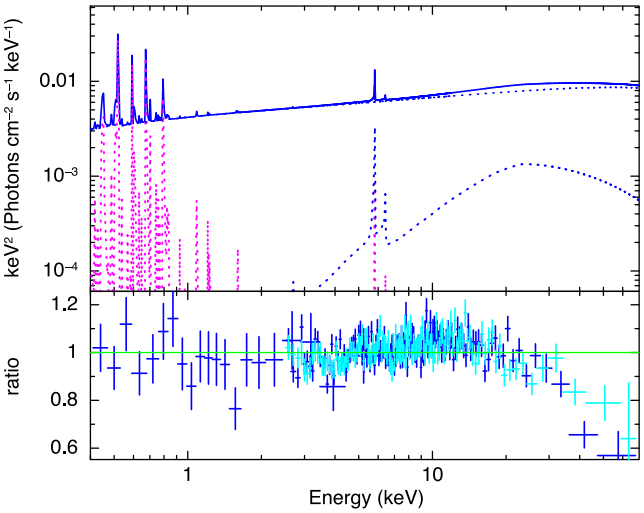

Figure 4. The initial fit to OPTXAGNF plus XILLVER to the *NuSTAR* and *Swift* data as described in Section 3.5. The model does not include intrinsic absorption, but does include OPTXAGNF (upper dashed blue line) a contribution from distant reflection quantified using XILLVER (lower dashed blue line) and soft band emission quantified using XSTAR (magenta dashed line). The *U*-band point is fitted in the model, but the X-ray data only are shown for clarity. The lower panel shows X-ray ratio residuals from FMPA and the XRT (dark blue) and from FPMB (aqua). Note the strong curvature present in the residuals to the *NuSTAR* data.

is present which modifies the continuum, producing the hard spectral shape between 2 and 10 keV, while reproducing the underlying steep UV to soft X-ray and also hard X-ray continuum which is apparent in the overall SED shape. To test the former, we modified the OPTXAGNF continuum to include an additional ad hoc exponential cut-off in the *NuSTAR* bandpass below 100 keV, while the cut-off value for the reflection model was also tied to that of the illuminating continuum for consistency. While this did result in a good statistical description of the *Swift* plus *NuSTAR* data (954/952), the resulting continuum shape now has an even harder photon index of $\Gamma = 1.65 \pm 0.03$ with a very low value for the exponential cut-off of $E_{\rm cut} = 52 \pm 9$ keV. Such an extreme hard X-ray continuum shape is flatter than that produced by standard Comptonization models, although a flat spectrum is predicted for coronae that have a significant bulk velocity (Sobolewska & Papadakis 2009).

Investigating this further (and dropping the additional model cut-off), a single layer of ionized absorption was added to the model to modify the OPTXAGNF continuum, using the ZXIPCF model (Reeves et al. 2008). Complex absorption is expected in this source, as a multizoned X-ray absorber is seen in X-ray grating data (Di Gesu et al. 2013), and has been invoked to explain the X-ray spectral variability observed during the *XMM* observations (Pounds et al. 2004a,b; Turner & Miller 2009). The existence of a significant outflowing X-ray absorber is supported by the unambiguous evidence for a disc wind, seen in UV and X-ray spectra of this AGN (Dunn et al. 2007; Di Gesu et al. 2013).

We allow the column density, ionization, and covering fraction of the absorber to vary, this model represents the clumpy absorber favoured by recent observations (see Introduction). ZXIPCF assumes a $\Gamma = 2.2$ illuminating spectral form over 1–1000 Ryd. The intrinsic continuum (underlying the reprocessor) appears to be close to this photon index, although, of course, the observed continuum is often much harder owing to the effects of reprocessing. As the absorber is likely illuminated predominantly by the intrinsic continuum, the assumed SED for ZXIPCF is reasonable for application to this source.

For consistency, the ionization parameter of the reflector was tied to that of the absorber, assuming they arise from the same material. This yielded a very good fit ($\chi^2 = 942/952$ degrees of freedom), with values of $N_{\rm H} = 3.1 \pm 0.3 \times 10^{23}$ cm^{-2}, $\log \xi = 0.9 \pm 0.3$ erg cm s^{-1}, and $f_{\rm cov} = 0.37 \pm 0.03$ for the absorber. Now the photon index is steeper, with $\Gamma = 2.0$ and that, plus the effect of the continuum curvature imparted by the absorber above 2 keV combined with the (modest) ∼100 keV rollover intrinsic to the OPTXAGNF model, is able to reproduce the shape of the hard X-ray spectrum seen in the *NuSTAR* data. For this model, the absorption correction is about 60 per cent in the 2–10 keV band, yielding an absorption-corrected luminosity $L_{2\text{–}10,\,\rm int} = 6.7 \times 10^{44}$ erg s^{-1}.

3.6 Spectral variability

Any acceptable model must also account for the spectral variability exhibited between epochs. First, we consider all the broad-band X-ray data by adding existing 2007 and 2010 *Suzaku* data sets to the fit, linking parameters between the epochs and then allowing variations of individual parameters, in turn, to account for the spectral and flux variability. We tried several variations of this fit, as follows:

(i) The first model comprised OPTXAGNF plus XILLVER, with no absorption zones. The model parameters were linked, allowing only $\frac{L}{L_{\rm Edd}}$ to vary between epochs. A poor fit was obtained, with $\chi^2 = 1862/1319$ degrees of freedom and a hard photon index, $\Gamma = 1.79 \pm 0.01$, failing to account for the clear spectral curvature and rollover in the hard band (Fig. 5, top panel).

(ii) Taking the model from (i), we allowed more freedom in that by letting τ vary between epochs, which has a strong effect on the models ability to account for the soft excess. This extra freedom resulted in a better fit, with $\chi^2 = 1585/1316$ degrees of freedom, however it did not account for the high-energy rollover in the data (Fig. 5, panel 2)

(iii) A single zone of partial covering absorption was added to the joint fit, using ZXIPCF as previously described. In this fit, τ was linked rather than allowed to vary between epochs, $\frac{L}{L_{\rm Edd}}$ was allowed to vary between epochs. This improved the fit, giving $\chi^2 = 1433/1312$ degrees of freedom. This somewhat improves the fit to the hard band, and the underlying continuum steepens to $\Gamma = 1.92 \pm 0.02$ (Fig. 5, panel 3)

(iv) A second zone of absorption was added to the model using a second ZXIPCF component. Application of the 'two-zone' absorber model to the 2015 *NuSTAR* and *Swift* data alone, provides a good fit with $\chi^2 = 925/945$ degrees of freedom (Table 1, column 3). This zone improves the fit further for the *NuSTAR/Swift* plus *Suzaku* data, giving $\chi^2 = 1291/1309$ degrees of freedom and this provides the first acceptable parametrization of the hard X-ray data (Fig. 5, bottom panel). The underlying photon index has now steepened to $\Gamma = 2.00 \pm 0.03$ (Table 1, column 4).

In conclusion, the broad-band X-ray spectrum revealed by *NuSTAR* and *Suzaku* requires two absorption zones, one of which must be a high column of gas, for the spectral curvature to be modelled correctly. With that in place, the continuum index is required to be steeper, and together these and the intrinsic rollover present in the OPTXAGNF model allow a good match between data and the model above 20 keV. Detailed interpretation of the soft band changes is more ambiguous. In the absence of grating data, we cannot distinguish a variable soft excess (that we have

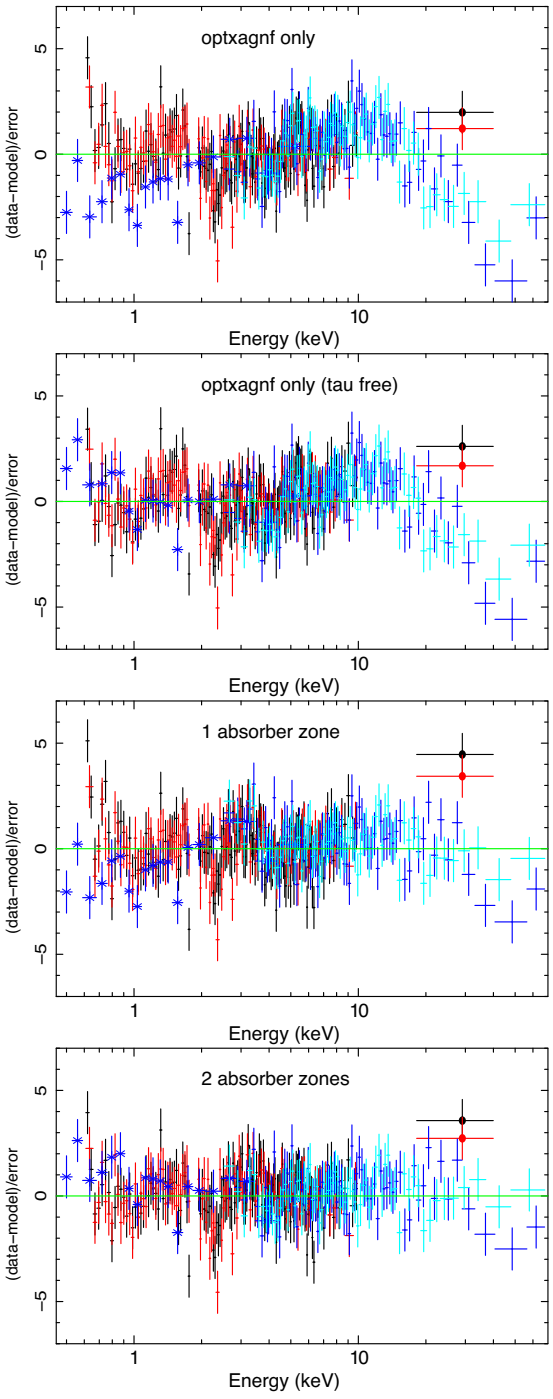

Figure 5. Residuals: joint fits to *NuSTAR* (FPMA dark blue, FPMB aqua)/*Swift*(dark blue cross) and *Suzaku* data (2007 black, 2010 red) using the OPTAXAGNF model. Parameters were free but linked between epochs, see Section 3.6 and Table 1 for details. First, only a colourless continuum variability (via the fraction $\frac{L}{L_{\rm Edd}}$) was allowed between epochs (top) with no intrinsic absorption included. Then, the optical depth of the warm corona (τ) was allowed to vary between epochs (panel 2). Significant residuals are still present in the spectra that are unaccounted for in the bare coronal continuum model. Following this a single zone of absorption was allowed in the fit (panel 3), with covering fraction allowed to vary between epochs. Finally, two zones of absorption were allowed (bottom), accounting for the remaining residuals. Note: due to the lower S/N and higher systematics of the non-imaging *Suzaku* PIN data, these have been binned to a single 15-40 keV flux point.

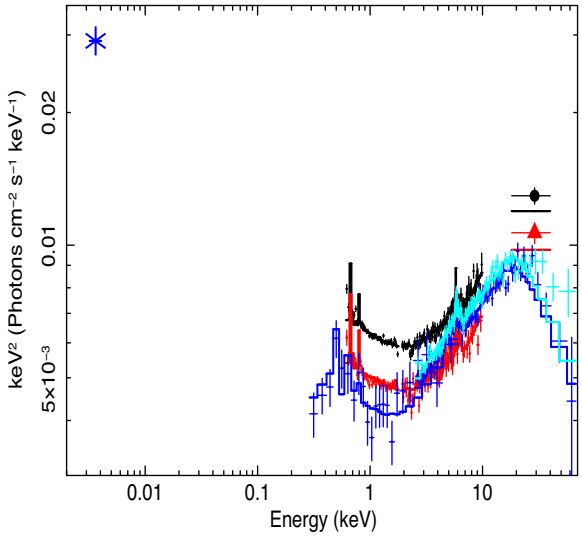

Figure 6. Unfolded data versus the best-fitting multiepoch OPTXAGNF model from Table 1: symbols as for Fig. 5. Note that for the *Suzaku* PIN data, the model is corrected for the calibration cross normalization factor (relative to XIS), but the data are not corrected.

parametrized here by varying τ) or a variable soft-band absorber (cf. Di Gesu et al. 2014).

3.7 The two-zone absorber model applied across all flux states

Having established a need for two absorber zones modifying the OPTXAGNF continuum, we now consider testing that model across all flux states. We note that between the 2007 and 2010 *Suzaku* observations there is no significant difference in spectral shape, although there is a 'colourless' component of variability (i.e. a simple flux change) between those epochs. That flux change cannot be ascribed to changes in the absorbing gas zones in the model, but is likely a change in the underlying continuum level, therefore model parameters (Table 1) were linked to implement that. In OPTXAGNF, a simple flux change can be described in a number of ways, allowing the Eddington ratio, Comptonized fraction or coronal radius to vary. As there is degeneracy in the continuum model, we selected to parametrize this long time-scale flux change by allowing only the Eddington ratio to vary between those two epochs (i.e. this is not a unique solution for the source).

Table 1 shows the fits, with the parameters linked between the epochs, except for absorber covering fractions and the Eddington ratio (Table 1, columns 4–6). The ionization of the reflector was linked to the highest column absorber (zone 1 in Table 1). Zone 1 is of sufficiently high column density that it may produce the weak observed scattered spectral component. However, we cannot rule out a contribution to the scattered spectral component from other, higher column-density gas. The column densities and ionization states of the two absorbers were linked for all data sets, allowing only the covering fraction to vary. For the two *Suzaku* epochs, we linked the absorber parameters (owing to the lack of any change in spectral shape between 2007 and 2010). Obviously, the lack of high-quality *NuSTAR* data for all epochs limits the test of parameter variability across the different flux states, and limits us to a parametrization, rather than a unique solution to the problem. This joint fit yielded $\chi^2 = 1432/1312$ degrees of freedom, with the best spectrum shown over the UV to hard X-ray range in Fig. 6. The model is also shown in Fig. 7, corrected for absorption to show the intrinsic form.

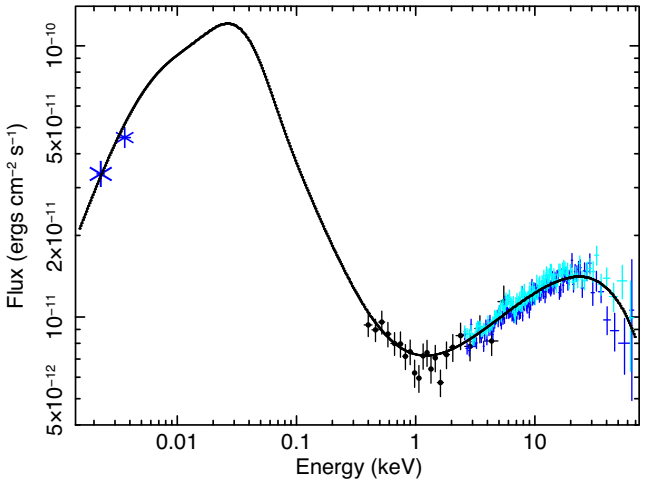

Figure 7. The fitted OPTXAGNF continuum model to 2015 *NuSTAR* and *Swift* data (Table 3, column 4, colours as for Fig. 1). Galactic and intrinsic absorption and host reddening have been removed to show the intrinsic disc plus coronal emission from OPTXAGNF. Overlaid on this are the X-ray data points, corrected for absorption (Galactic and intrinsic) and the UVOT U and V points corrected for Galactic reddening. The UVOT U point was fitted to the data, while the V point (far left) was not included in the fit (because of a concern about its lack of simultaneity, see the text for details), but is overlaid for comparison. For visual clarity, the XSTAR emission and XILLVER model components are not shown as these make only a small energetic contribution to the broad emission).

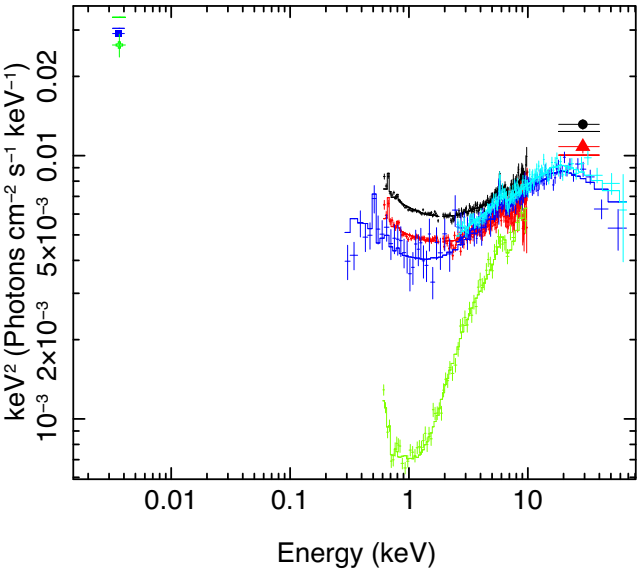

Figure 8. The *NuSTAR* (blue and aqua) plus simultaneous Swift XRT and UVOT data (blue) compared to the flux states sampled by previous *XMM* (pn and OM *U*-band as green, 2002) and *Suzaku* (black is 2007, red is 2010) observations. The solid line is the best-fitting model corresponding to Table 1. Note that the low flux *XMM* epoch is much more heavily absorbed.

In order to establish whether our general model is capable of accounting for all flux states – in addition to explaining the *NuSTAR/Swift* data and the *Suzaku* data, the model should be able to extrapolate to any extreme flux states exhibited by the target. Therefore, we added to our consideration the extreme low flux X-ray state observed using *XMM* (Pounds et al. 2004a; Di Gesu et al. 2014). Previous work on those *XMM* data from the low state shows clear evidence for a variable soft X-ray absorber (Pounds et al. 2004b; Di Gesu et al. 2014), and this historical knowledge adds strong support for the two-zone absorption model to account for the variability over all epochs. The inclusion of the *XMM* data produces a fit with $\chi^2 = 2296/1643$ degrees of freedom, providing a poor match to the shape of the lowest flux state from 2002. Considering the evidence to date (e.g. Pounds et al. 2004b) for changes in the opacity of the absorber, we freed the absorber parameters in turn for the *XMM* epoch, and refit. Freeing the column and ionization of both absorber layers for 2002 data (as well as the covering fraction) produced a significant improvement over the simpler alternatives. With the absorber zones completely free for 2002 data (Table 1, column 7), we achieved a joint fit statistic $\chi^2 = 1857/1634$ degrees of freedom (Fig. 8). Indeed, it is apparent from the figure that the *XMM* low state spectrum has a substantially harder spectrum, with pronounced absorption seen below 10 keV. Much of the absorption change is driven by an increase in absorber covering for the two zones (see Table 1).

4 DISCUSSION

We have analysed new data from simultaneous *NuSTAR* and *Swift* observations of 1H 0419-577 during 2015, in conjunction with previous *Suzaku* observations from 2007 and 2010 and an *XMM* observation (Pounds et al. 2004a; Di Gesu et al. 2014) that sampled the extreme low X-ray flux state exhibited during 2002. Consideration of the new *NuSTAR* data appear to rule out a contribution from strong disc reflection, both due to the shape of the high-energy spectrum above 10 keV and the lack of a strong broad Fe K α line.

Spectral analysis of the *NuSTAR*, *Swift* and *Suzaku* data shows that the source can be fitted with a multitemperature accretion disc, shrouded with a complex clumpy absorber. This model includes both absorption effects and a scattered light component and is consistent with some of the signatures of variability observed in this target. Adequate parametrization of the very lowest flux state requires changes in the absorber column and ionization state. The source shows a marked turnover at ~20 keV, that is adequately parametrized by the combined effects of the rollover at 100 keV in OPTXAGNF, the effects of the reprocessor and the $\Gamma \sim 2$ index recovered when all reprocessing effects are modelled. We cannot rule out the presence of a cut-off in the primary continuum form associated with the high energy corona. Application of this model has allowed us to isolate a colourless component of variability effective over time-scales of years, that is consistent with changes in the accretion flow on small radial scales in the inner disc.

4.1 The XUV continuum

We have analysed new data from simultaneous *NuSTAR* and *Swift* observations of 1H 0419-577 during 2015, finding a remarkably low turnover energy in the hard spectrum. As detailed in Section 3.3, in the context of pure Comptonizing corona models, this marked turnover would imply an electron temperature, $kT \sim 15$ keV, for the accretion disc, similar to the value reported for Ark 564 (Kara et al. 2017), and lower than that reported for GRS1734-292 (Tortosa et al. 2017) (also see Tortosa et al. 2018).

In order to solidify our identification of the most compelling modelling solutions, we consider further the implications of the Comptonization model presented in Section 3.3, and in particular the possibility of a low-temperature corona in 1H 0419-577. Following Fabian et al. (2015) (and also Dove et al. 1987, Svensson 1987, Lightman & Zdziarski 1987) and taking the coronal radius as

$R = R_{\rm cor} = 15 r_{\rm g}$ and the fitted Eddington ratio $\frac{L}{L_{\rm Edd}} \sim 0.4$, we estimated the source compactness as $l \sim 600$. Assuming kT = 15 keV (Section 3.3), we calculated the source temperature $\Theta = \frac{kT}{m_{\rm e}c^2} = 0.03$. Comparing this with the distribution of Fabian et al. (2015, their fig. 2) shows 1H 0419-577 to be outside of the range observed for AGN in the Fabian et al. (2015) sample. Thus, it appears that 'pure' Comptonization models may not yield meaningful results for the cut-off: this led us to try alternative models where at least some of the high-energy curvature can be produced by a higher column partial-covering absorber.

Note that in contrast to 1H 0419-577, the low black hole mass of the Narrow Line Seyfert 1 Ark 564 has both a very soft SED, which peaks in the EUV and soft X-rays (Romano et al. 2004) and a steep X-ray photon index, where $\Gamma \sim 2.6$ (Giustini et al. 2015). This might result in substantial Compton cooling of the high-energy electron pair population, leading to an unusually cool coronal temperature. Furthermore, as noted by Kara et al. (2017), the presence of a hybrid (thermal/non-thermal) plasma (Zdziarski, Lightman & Maciolek-Niedzwiecki 1993; Fabian et al. 2017) could then still maintain a pair-dominated plasma, despite the low electron temperature. On the other hand, in 1H 0419-577 the black hole mass is likely two orders of magnitude higher than in Ark 564, leading to an SED peaked in the optical/UV, while the apparently harder photon index (of $\Gamma \sim 1.7$) below 10 keV, (if the effect of absorption is not accounted for in the continuum modelling) may not be able to easily cool the high-energy electron population. Thus at least at first sight, 1H 0419-577 might appear to be a less plausible AGN for which such a low temperature plasma could be maintained. Indeed in 1H 0419-577, the cut-off energy and subsequent coronal temperature depends on the continuum model adopted. In the reflection fits (section 3.4), the cut-off energy increases to 60 keV. Furthermore, when any partially covering absorption is accounted for (Section 3.5), then the data are consistent with the 100 keV coronal temperature assumed in the OPTXAGNF model.

We have found that the broad-band XUV continuum, sampled using simultaneous *Swift* and *NuSTAR* data, can be modelled using a colour-corrected accretion disc while hard X-rays arise via Compton up-scattering from a putative corona (Done et al. 2012). The observation of a colourless component of flux change, most evident between 2007 and 2010, indicates the need for continuum variability in addition to the absorber variations. Recent work by Di Gesu et al. (2014) presented an alternative, but phenomenologically similar model for the UV to X-ray continuum, based upon contemporaneous *XMM* and *HST* observations of 1H 0419-577: their parametrization was based around a nested double-Comptonization model. Consistent with previous modelling, we find the continuum to be modified by reprocessing in two layers of partial-covering gas, including a Compton-thick layer that is consistent with producing the weak Fe Kα line observed. This X-ray absorber imprints a spectral and time variability signature on the data in addition to that imposed by the continuum variation.

The Eddington ratio derived from the fit to OPTXAGNF is ∼0.4 (Table 1) and this can be related to the viscous time-scale. The viscous time-scale is a characteristic time-scale of the mass flow, i.e. the ratio of the radius of the perturbation in flow to the radial velocity. To achieve observable modulation of the X-ray continuum flux from changes in the Eddington ratio, viscosity changes, or accretion rate changes have to propagate inwards by a significant radial distance and cause fluctuations of mass accretion rate in a region of significant energy release. This is only possible for fluctuations on time-scales at or exceeding the viscous time-scale at the radius where fluctuations are manifested in the accretion flow. We consider the simple colourless flux variability observed between 2007 and 2010. For an AGN with a supermassive black hole of mass $10^8\,{\rm M}_\odot$, operating at an Eddington ratio of 0.4, interpretation of a ∼900 d variability time-scale as a viscous time-scale, yields a radius $\sim 10\, r_{\rm g}$ for the fluctuations in the accretion flow (Czerny 2004).

4.2 The X-ray absorber

The absorber complex is very important in shaping the spectral and timing behaviour of 1H 0419-577. Previous work by Pounds et al. (2004a) and Di Gesu et al. (2014) interpreted spectral variability below 10 keV as changes in the X-ray absorber, finding that when the source brightened the opacity of this absorber decreased, consistent with an increase in gas ionization state. Turner et al. (2009) found evidence in *Suzaku* data for a Compton thick component of absorption, extending the Pounds et al. (2004a) and Di Gesu et al. (2014) model to higher energies. Turner et al. (2009) discussed how the gas may be part of a disc wind, and estimated a 10 per cent global covering for the Compton-thick zone of gas, based on the Fe Kα luminosity, and a wind opening angle $\simeq 12^\circ$. We have applied a new variation on the X-ray model, based upon new broad-band data, and while this has resulted in different parameter values than those found either by Pounds et al. (2004a) or Turner et al. (2009), our results are in agreement with those previous frameworks: a multizoned absorber is required to explain the range of behaviour exhibited by 1H 0419-577 in the X-ray regime. The spectral variability between epochs could be either explained by variations in the absorber covering fraction and/or column density. However, as there is only one *NuSTAR* epoch with high quality hard X-ray data available, for simplicity we chose to tie the column densities while allowing the covering fraction to vary. This is not a unique solution.

There are several compelling lines of evidence that indicate the X-ray absorber to be part of a complex outflow of material: Tombesi et al. (2011) report Fe XXVI *Ly*α and Fe XXV absorption from gas outflowing at ∼24 000 km s^{-1}, while Di Gesu et al. (2013) detail an absorber that has signatures across the UV and soft X-ray regimes, with several kinematic components evident in the UV data, tracing outflow components over 38–220 km s^{-1} (as previously observed in other UV spectra of this AGN, e.g. Dunn et al. 2007).

For a black hole of mass $3.8 \times 10^8\,{\rm M}_\odot$, $1\, r_{\rm g}$ is approximately 10^{14} cm. Assuming the continuum source size to be of order $10\, r_{\rm g}$, for 1H 0419-577 that is a size of $\sim 10^{15}$ cm. Under an assumption that the cloud size is at least the size of the continuum source (similar, for example, to NGC 1365, Risaliti et al. 2007; Braito et al. 2014) then for the clouds we have $\Delta R \sim 10\, r_{\rm g} \sim 10^{15}$ cm. The cloud density, $n_{\rm e}$, can then be estimated from the column density, $N_{\rm H}$ in the fit, and the radial extent, using $N_{\rm H} = n_{\rm e} \times \Delta R$, which yields $n_{\rm e} \sim 10^9 {\rm cm}^{-3}$ for the thick clouds in zone 1. The radial distance of the zone can then be derived from using this density estimate and the definition of ionization parameter (see Section 3.3) to give a radial distance $r_{z1} \sim 10^{18}$ cm from the illuminating source. We note that this is simply an order-of-magnitude estimate. The scale of the optical broad-line region gas in this source is $r_{\rm BLR} \sim 10^{17}$cm (Guainazzi et al. 1998) and so the thick absorbing zone is consistent with the outer broad line region or the putative clumpy torus. However, the time-scale on which changes in covering fraction are observed in this and other AGN (e.g. Pounds et al. 2004b; Risaliti et al. 2007; Bianchi, Maiolino & Risaliti 2012) suggests a location on sub-pc scales to be more plausible than very extended kpc scales

(such as that found for the lower column soft X-ray emitting gas Di Gesu et al. 2013, 2017).

Di Gesu et al. (2013) conclude that a low-ionization absorbing gas zone measured during the 2010 XMM observations must exist at radii >3 kpc from the nucleus, i.e. on a much larger scale than either of the absorber zones detailed here, possibly associated with the galaxy interstellar medium. It is not clear that the high-column clumps in our model are required to be co-spatial with the lower column gas. Di Gesu et al. (2017) find evidence of large-scale, geometrically thin, X-ray line emitting gas in *Chandra* imaging data. That gas exists on scales of several kpc from the nucleus. One possible origin they suggest is gas that is shock-heated by a wind, on larger scales. We find the high-column component of the X-ray gas to be clumpy and highly variable on time-scales of months–years (Pounds et al. 2004a,b) – this component therefore is likely closer in to the nucleus (perhaps on the pc or sub-pc scale) than the other X-ray absorbing zones. One possible link is that the inner X-ray wind, for instance as is predicted in radiatively driven wind simulations such as in Sim et al. (2010), is driving the gas out to larger scales and seen in the form of the larger scale outflow in the *Chandra* and [O III] images. It seems likely that the various absorbers (Di Gesu et al. 2013) found in this AGN form part of a multiphase outflow. Some of the broad Fe Kα features in AGN could arise from the forward-scattered emission from such a wind and indeed, existing broad Fe K components in a small sample of unobscured AGN have been found to be for consistent with the line profiles predicted by the Sim et al. (2010) model (Tatum et al. 2012).

5 CONCLUSIONS

We have analysed and modelled spectral data from a simultaneous *NuSTAR* and *Swift* observation of 1H 0419-577 during 2015. The broad-band spectral form shows a pronounced turnover around 20 keV. We have shown that the rollover cannot be due only to the presence of a strong Compton hump: instead it is likely due to both the presence of thermal Comptonization producing the high-energy spectrum and the modifying effects of absorption on the overall broad spectrum, the latter also producing a steeper-than-observed intrinsic continuum once accounted for in the spectral modelling.

The broad-band continuum form can be modelled using a centre-corrected accretion disc around a maximally spinning black hole. In the context of this model, hard X-rays are produced via Compton up-scattering in a corona having $\tau \sim 5$. Multiple epochs of X-ray data from *Suzaku* and *NuSTAR*/*Swift* show that flux variations on time-scales of years are consistent with modest changes in the source Eddington ratio, likely attributable to fluctuations in the inner disc flow, around $10\,r_{\rm g}$. The models tested here are not unique representations of the variability – alternatives such as changes in the Comptonizing corona cannot be ruled out – but our analysis showcases some of the simple and interesting possibilities to explain these data.

ACKNOWLEDGEMENTS

TJT acknowledges NASA grant NNH13CH63C. JNR acknowledges NASA grant NNX15AV18G. We are grateful to the *NuSTAR* operations team for performing this observation and providing software and calibration for the data analysis. We thank the anonymous referee for comments which improved this manuscript. This research has also made use of data obtained from the High Energy Astrophysics Science Archive Research Center (HEASARC), provided by NASA's Goddard Space Flight Center and from the NASA/IPAC Extragalactic Database (NED), which is operated by the Jet Propulsion Laboratory, California Institute of Technology, under contract with NASA.

REFERENCES

Alonso-Herrero A., et al., 2011, ApJ, 736, 82
Antonucci R., 1993, ARA&A, 31, 473
Asensio Ramos A., Ramos Almeida C., 2009, ApJ, 696, 2075
Asensio Ramos A., Ramos Almeida C., 2013, MNRAS, 428, 195
Bentz M. C., Peterson B. M., Netzer H., Pogge R. W., Vestergaard M., 2009, ApJ, 697, 160
Bianchi S., Maiolino R., Risaliti G., 2012, Adv. Astron., 2012, 782030
Braito V., Reeves J. N., Gofford J., Nardini E., Porquet D., Risaliti G., 2014, ApJ, 795, 87
Burrows D. N., et al., 2005, Space Sci. Rev., 120, 165
Burtscher L., et al., 2016, A&A, 586, A28
Cardelli J. A., Clayton G. C., Mathis J. S., 1989, ApJ, 345, 245
Czerny B., 2004, preprint (arXiv:astro-ph/0409254)
Dadina M., 2008, A&A, 485, 417
Dauser T., García J., Parker M. L., Fabian A. C., Wilms J., 2014, MNRAS, 444, L100
Deluit S., Courvoisier T. J.-L., 2003, A&A, 399, 77
et al.Di Gesu L., 2013, A&A, 556, A94
Di Gesu L., Costantini E., Piconcelli E., Ebrero J., Mehdipour M., Kaastra J. S., 2014, A&A, 563, A95
Di Gesu L., Costantini E., Piconcelli E., Kaastra J. S., Mehdipour M., Paltani S., 2017, A&A, 608, 10
Done C., Davis S. W., Jin C., Blaes O., Ward M., 2012, MNRAS, 420, 1848
Dove J. E., Rusk A. C. M., Cribb P. H., Martin P. G., 1987, ApJ, 318, 379
Dunn J. P., Crenshaw D. M., Kraemer S. B., Gabel J. R., 2007, AJ, 134, 1061
Elitzur M., Shlosman I., 2006, ApJ, 648, L101
Fabian A. C., Miniutti G., Iwasawa K., Ross R. R., 2005, MNRAS, 361, 795
Fabian A. C., Lohfink A., Kara E., Parker M. L., Vasudevan R., Reynolds C. S., 2015, MNRAS, 451, 4375
Fabian A. C., Lohfink A., Belmont R., Malzac J., Coppi P., 2017, MNRAS, 467, 2566
García J., Dauser T., Reynolds C. S., Kallman T. R., McClintock J. E., Wilms J., Eikmann W., 2013, ApJ, 768, 146
García J. et al., 2014, ApJ, 782, 76
Giustini M., Turner T. J., Reeves J. N., Miller L., Legg E., Kraemer S. B., George I. M., 2015, A&A, 577, A8
Guainazzi M., et al., 1998, A&A, 339, 327
Harrison F. A., et al., 2013, ApJ, 770, 103
Kara E., García J. A., Lohfink A., Fabian A. C., Reynolds C. S., Tombesi F., Wilkins D. R., 2017, MNRAS, 468, 3489
Koyama K., et al., 2007, PASJ, 59, 23
Lightman A. P., Zdziarski A. A., 1987, ApJ, 319, 643
Mehdipour M., et al., 2011, A&A, 534, A39
Miller L., Turner T. J., 2013, ApJ, 773, L5
Miniutti G., Fabian A. C., 2004, MNRAS, 349, 1435
Mitsuda K., et al., 2007, PASJ, 59, 1
Mizumoto M., Ebisawa K., Sameshima H., 2014, PASJ, 66, 122
O'Neill P. M., Nandra K., Papadakis I. E., Turner T. J., 2005, MNRAS, 358, 1405
Page K. L., Pounds K. A., Reeves J. N., O'Brien P. T., 2002, MNRAS, 330, L1
Pal M., Dewangan G. C., 2013, MNRAS, 435, 1287
Pal M., Dewangan G. C., Kembhavi A. K., Misra R., Naik S., 2017, MNRAS, 473, 3584
Petrucci P. O., et al., 2001, ApJ, 556, 716
et al.Porquet D., 2017, A&A, 609, 17
Pounds K. A., Nandra K., Stewart G. C., George I. M., Fabian A. C., 1990, Nature, 344, 132

Pounds K. A., Reeves J. N., Page K. L., O'Brien P. T., 2004a, ApJ, 605, 670
Pounds K. A., Reeves J. N., Page K. L., O'Brien P. T., 2004b, ApJ, 616, 696
Proga D., Kallman T. R., 2004, ApJ, 616, 688
Ramos Almeida C., Alonso-Herrero A., Levenson N. A., Asensio Ramos A., Rodríguez Espinosa J. M., González-Martín O., Packham C., Martínez M., 2014, MNRAS, 439, 3847
Reeves J., Done C., Pounds K., Terashima Y., Hayashida K., Anabuki N., Uchino M., Turner M., 2008, MNRAS, 385, L108
Ricci C., Beckmann V., Audard M., Courvoisier T. J.-L., 2010, A&A, 518, A47
Risaliti G., Elvis M., Fabbiano G., Baldi A., Zezas A., Salvati M., 2007, ApJ, 659, L111
Romano P., et al., 2004, ApJ, 602, 635
Roming P. W. A., et al., 2005, Space Sci. Rev., 120, 95
Różańska A., Malzac J., Belmont R., Czerny B., Petrucci P.-O., 2015, A&A, 580, A77
Sim S. A., Proga D., Miller L., Long K. S., Turner T. J., 2010, MNRAS, 408, 1396
Sobolewska M. A., Papadakis I. E., 2009, MNRAS, 399, 1597
Svensson R., 1987, MNRAS, 227, 403
Takahashi T., et al., 2007, PASJ, 59, 35
Tatum M. M., Turner T. J., Sim S. A., Miller L., Reeves J. N., Patrick A. R., Long K. S., 2012, AJ, 752, 9
Tatum M. M., Turner T. J., Miller L., Reeves J. N., 2013, ApJ, 762, 80
Terashima Y., et al., 2009, PASJ, 61, 299
Thomas A. D., Groves B. A., Sutherland R. S., Dopita M. A., Kewley L. J., Jin C., 2016, ApJ, 833, 266
Titarchuk L., 1994, ApJ, 434, 570
Tombesi F., Cappi M., Reeves J. N., Palumbo G. G. C., Braito V., Dadina M., 2011, ApJ, 742, 44
Tortosa A., et al., 2017, MNRAS, 466, 4193
Tortosa A., Bianchi S., Marinucci A., Matt G., Petrucci P. O., 2018, preprint (arXiv:1801.04456)
Turner T. J., Miller L., 2009, A&A Rev., 17, 47
Turner T. J., Miller L., Kraemer S. B., Reeves J. N., Pounds K. A., 2009, ApJ, 698, 99
Walton D. J., Reis R. C., Fabian A. C., 2010, MNRAS, 408, 601
Walton D. J., Nardini E., Fabian A. C., Gallo L. C., Reis R. C., 2013, MNRAS, 428, 2901
Zdziarski A. A., Lightman A. P., Maciolek-Niedzwiecki A., 1993, ApJ, 414, L93
Zdziarski A. A., Johnson W. N., Magdziarz P., 1996, MNRAS, 283, 193
Życki P. T., Done C., Smith D. A., 1999, MNRAS, 309, 561

This paper has been typeset from a TEX/LATEX file prepared by the author.